High-spin collective structures in doubly-odd ^{114}Sb

E.S. Paul

Oliver Lodge Laboratory, University of Liverpool, P.O. Box 147, Liverpool L69 3BX, United Kingdom

V.P. Janzen

Chalk River Laboratories, AECL Research, Chalk River, Ontario, Canada K0J 1J0
and Department of Physics & Astronomy, McMaster University, Hamilton, Ontario, Canada L8S 4M1

D.C. Radford and D. Ward

Chalk River Laboratories, AECL Research, Chalk River, Ontario, Canada K0J 1J0

S.M. Mullins

Department of Physics & Astronomy, McMaster University, Hamilton, Ontario, Canada L8S 4M1

D.B. Fossan, D.R. LaFosse, H. Schnare, H. Timmers, and P. Vaska

Department of Physics, State University of New York at Stony Brook, New York 11794

R.M. Clark and R. Wadsworth

Department of Physics, University of York, Heslington, York YO1 5DD, United Kingdom

(Received 13 April 1994)

Several collective rotational bands have been established in doubly-odd ^{114}Sb extending to high spin ($\sim 35\hbar$) and excitation energy (~ 18 MeV). Two pairs of strongly coupled negative-parity sequences were observed at low spin consisting of stretched quadrupole transitions and interlinking $M1$ dipole transitions. These bands are interpreted in terms of the $\pi[404]9/2^+$ orbital. A third pair of signature-partner bands was established; however, no interlinking $M1$ transitions were observed in this case. These bands are associated with the $\pi[550]1/2^-$ intruder orbital, and the rotational properties are remarkably similar to those of a $\pi h_{11/2}$ "intruder" band in ^{113}Sb having enhanced quadrupole deformation ($\beta_2 \sim 0.32$). The experimental results are discussed with the aid of total Routhian surface and Woods-Saxon cranking calculations.

PACS number(s): 21.10.Re, 27.60.+j, 23.20.Lv

I. INTRODUCTION

Nuclei bordering on the spherical closed shell at $Z=50$ have shown exotic collective structures, which coexist with the expected single-particle properties. The existence of collective rotational structures in the even tin ($Z=50$) isotopes has been known for some time (e.g., Ref. [1]). Furthermore, many rotational cascades have recently been established to high spin ($I \sim 40\hbar$) in several odd-A antimony ($Z=51$) isotopes ranging from ^{109}Sb to ^{117}Sb [2–6]. Similar bands have now been established in several isotopes with $49 \leq Z \leq 53$ [7–11]. The unexpected collectivity in these isotopes, which are essentially spherical in their ground states, is derived from deformed 2-particle–2-hole ($2p$-$2h$) 0_2^+ states $\pi\{g_{7/2}^2 \otimes g_{9/2}^{-2}\}$ in the even tin core nuclei [12]. In addition, occupation of the strongly β-sloping $\pi[550]1/2^-$ "intruder" orbital, from the $\pi h_{11/2}$ subshell above the $Z = 50$ shell gap, is able to stabilize enhanced quadrupole shapes in a manner similar to the $\nu[660]1/2^+$ intruder orbital for $A \sim 135$ nuclei [13]. Values of the nuclear quadrupole moment, deduced for several nuclei in this mass region from mean lifetime measurements of nuclear states, confirm well-deformed shapes for the intruder bands. For example,

such measurements for an intruder band in ^{113}Sb yield a quadrupole deformation $\beta_2 \sim 0.32$ [5]. Similar measurements for related bands in ^{109}Sb and ^{108}Sn suggest more modest nuclear deformations of $\beta_2 = 0.20$–0.25 [3,9].

The present paper concentrates on collective structures in the doubly odd $^{114}_{51}$Sb$_{63}$ nucleus, which are observed up to high spin ($\sim 35\hbar$) and excitation energy (~ 18 MeV). Previous work on the low-spin level structure of ^{114}Sb below an excitation energy of 4 MeV is presented in Ref. [14].

II. EXPERIMENTAL DETAILS

High-spin states in doubly odd ^{114}Sb were populated with the ^{96}Zr($^{23}Na,5n$)^{114}Sb reaction at a bombarding energy of 102 MeV. The target consisted of two self-supporting foils of ^{96}Zr (86% enrichment), each of nominal thickness 600 μg/cm^2. The ^{23}Na beam was provided by the Tandem Accelerator Superconducting Cyclotron (TASCC) facility at the Chalk River Laboratories of AECL Research. Coincident γ-γ data were acquired with the 8π spectrometer, which consists of 20 Compton-suppressed HPGe detectors plus a 71-element BGO inner ball calorimeter, which provides γ-ray sum-

energy, H, and fold, K, information. The gains of the HPGe detectors were matched off line with an [88]Y radioactive source, and adjusted on line for a recoil velocity $v/c = 1.65\%$. Data were written onto magnetic tape for events in which two or more suppressed HPGe detectors registered in prompt time coincidence with nine or more elements of the inner ball (fold $K \geq 9$). Under this condition, approximately 2.7×10^8 events were recorded on tape.

In the off-line analysis for [114]Sb ($5n$ channel), only events with a total sum energy $H \leq 12$ MeV were incremented into a symmetrized E_γ-E_γ matrix. This low sum-energy condition greatly suppressed events from the competing $4n$ evaporation channel into [115]Sb. In addition to standard γ-γ matrices, angular correlation matrices were constructed from the coincidence data for groups of HPGe detectors at angles of $\pm 37°$ and $\pm 79°$ with respect to the beam axis. From these matrices, intensity ratios $I_\gamma(37°-79°)/I_\gamma(79°-37°)$ were obtained by gating on quadrupole transitions. We used these angular intensity ratios to assist in the assignment of transition multipolarities using the method of directional correlation from oriented states (DCO) [15].

TABLE II. Gamma-ray energies, relative intensities (corrected for detector efficiency), and angular correlation data for transitions associated with bands 3 and 4 in [114]Sb.

E_γ (keV)[a]	I_γ (%)[b]	$\dfrac{I_\gamma(37°-79°)}{I_\gamma(79°-37°)}$	Assignment
560.1	21.9	—	—
597.3	21.2	—	—
639.9	64.5	1.2(2)	E2
740.0	99.7	1.1(1)	E2
821.1	≡ 100	0.9(1)	E2
899.2	101.1	1.0(1)	E2
969.2	87.6	0.9(1)	E2
1046.8	76.1	0.9(1)	E2
1135.4	53.7	1.1(1)	E2
1219.5	43.0	1.1(1)	E2
1280.3	32.7	1.3(2)	E2
1343.9	21.0	—	—
1390.0	5.1	—	—
1485.3	9.8	—	—
1702.0	4.0	—	—
1930	1.0	—	—

[a]Energies are estimated to be accurate to ± 0.3 keV, except those quoted as integers which are accurate to ± 1 keV.
[b]Errors on intensities are typically less than 5%. Band 4 carries $\sim 10\%$ of the channel intensity.

TABLE I. Gamma-ray energies, relative intensities (corrected for detector efficiency), and angular correlation data for transitions associated with bands 1 and 2 in [114]Sb.

E_γ (keV)[a]	I_γ (%)[b]	$\dfrac{I_\gamma(37°-79°)}{I_\gamma(79°-37°)}$	Assignment[c]
207.7	≡ 100	0.6(1)	$(9^- \rightarrow 8^-)$
309.2	88	0.5(1)	$(10^- \rightarrow 9^-)$
343.1	65	0.5(1)	$(11^- \rightarrow 10^-)$
372.4	39	0.6(1)	$(12^- \rightarrow 11^-)$
391.3	31	0.7(1)	$(13^- \rightarrow 12^-)$
428.2	29	0.5(1)	$(14^- \rightarrow 13^-)$
470.1	31	0.6(1)	$(15^- \rightarrow 14^-)$
506.9	49[d]	0.7(1)[d]	$(16^- \rightarrow 15^-)$
506.9	49[d]	0.7(1)[d]	$(18^- \rightarrow 17^-)$
515.6	23	0.6(1)	$(17^- \rightarrow 16^-)$
537	11	—	$(19^- \rightarrow 18^-)$
652.7	13	1.1(1)	$(11^- \rightarrow 9^-)$
716.1	16	0.9(1)	$(12^- \rightarrow 10^-)$
764.5	15	1.0(1)	$(13^- \rightarrow 11^-)$
820.2	18	1.1(1)	$(14^- \rightarrow 12^-)$
897.8	20	0.9(1)	$(15^- \rightarrow 13^-)$
976.2	26	1.2(1)	$(16^- \rightarrow 14^-)$
1021.6	33[d]	0.9(1)[d]	$(17^- \rightarrow 15^-)$
1021.6	33[d]	0.9(1)[d]	$(18^- \rightarrow 16^-)$
1044	6	—	$(19^- \rightarrow 17^-)$

[a]Energies are estimated to be accurate to ± 0.3 keV, except those quoted as integers which are accurate to ± 1 keV.
[b]Errors on intensities are typically less than 5%. Bands 1 and 2 carry $\sim 20\%$ of the channel intensity.
[c]The negative-parity assignment of this band is adopted from Ref. [14]. The present theoretical analysis, however, suggests positive parity; see text for discussion.
[d]Doublet, value given for both transitions.

III. LEVEL SCHEME OF [114]Sb

The high-spin level scheme of [114]Sb, deduced from this work, is presented in Fig. 1, where seven bands of stretched quadrupole transitions, characteristic of collective nuclear rotation, are labeled. Strong $\Delta I = 1$ transitions were observed interlinking bands 1/2 and bands 6/7. Measured transition energies, intensities, angular correlation ratios, and spin-parity assignments for these bands are listed in Tables I–IV. Figure 2 shows part of the low-spin structure of [114]Sb [14] including the decay of

TABLE III. Gamma-ray energies, relative intensities (corrected for detector efficiency), and angular correlation data for transitions associated with band 5 in [114]Sb.

E_γ (keV)[a]	I_γ (%)[b]	$\dfrac{I_\gamma(37°-79°)}{I_\gamma(79°-37°)}$	Assignment
585.0	38.1	—	—
691.2	101.1	0.9(1)	E2
782.7	≡ 100	1.2(1)	E2
871.6	90.4	1.0(1)	E2
945.9	67.1	0.9(1)	E2
1018.8	53.3	1.1(1)	E2
1101.2	42.7	0.9(1)	E2
1189.3	35.1	—	—
1276.4	24.3	—	—
1358.8	13.2	—	—
1454.1	7.7	—	—
1587.9	3.5	—	—

[a]Energies are estimated to be accurate to ± 0.3 keV, except those quoted as integers which are accurate to ± 1 keV.
[b]Errors on intensities are typically less than 10%. Band 5 carries $\sim 10\%$ of the channel intensity.
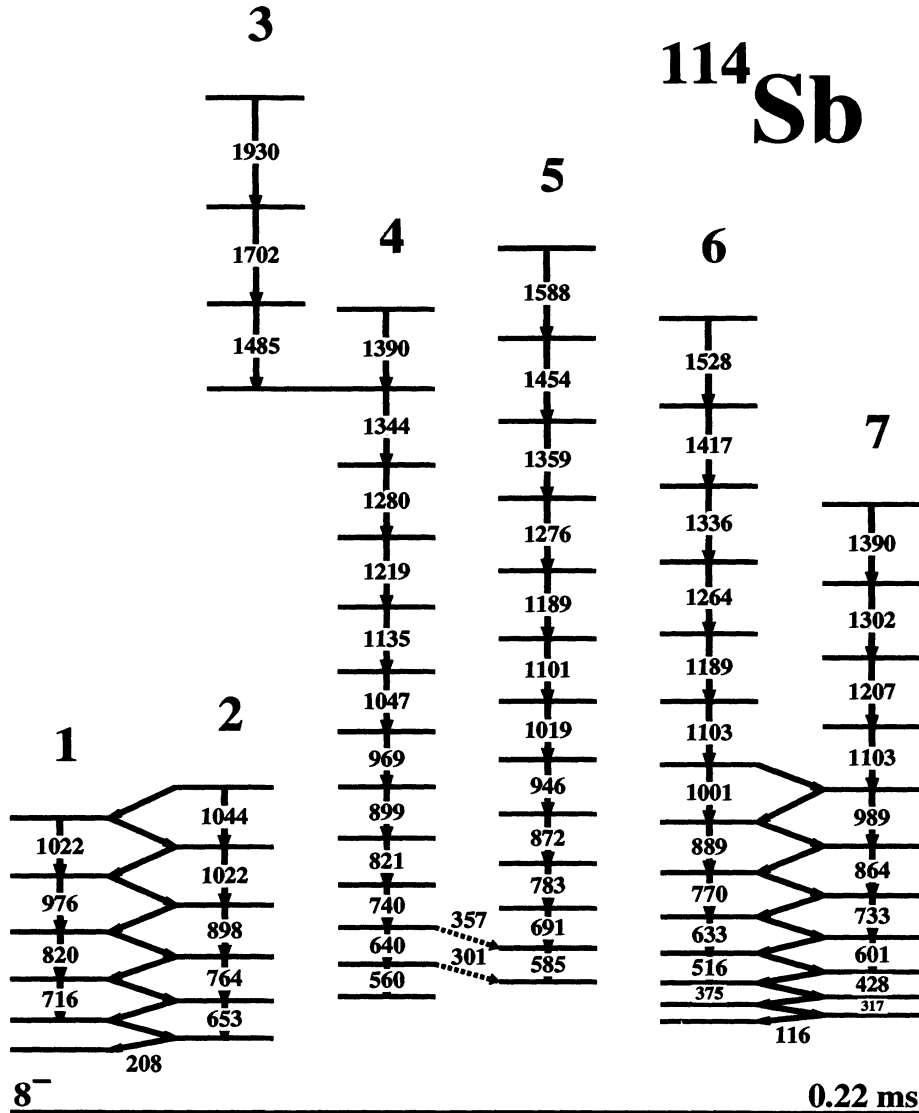
3

^{114}Sb

5

4

6

7

1930
1702
1485
1390
1588
1528
1390
1344
1454
1417
1302
1280
1359
1336
1207
1219
1276
1264
1103
1135
1189
1189
1047
1101
1103
989
969
1019
1001
864
946
889
733
899
872
770
601
821
783
633
428
740   357   691   516   317
640   301   585   375
560   116

1   **2**

1044
1022
1022
976
898
820
764
716
653
208

8$^-$ **0.22 ms**

FIG. 1. High-spin rotational bands in ^{114}Sb. Transition energies are given in keV. The lowest level of band 1 resides 1067 keV above the 8$^-$ isomeric level, while the lowest level of band 6 resides at 1577 keV above the isomer. The relative excitation energies of bands 4 and 5 are not known. For clarity, the energies of the interlinking dipole transitions of bands 1/2 and 6/7 are not labeled, except for the first transition in each case.

bands 6/7 into the known levels. The isomeric 8$^-$ state, shown at the bottom in Figs. 1 and 2, decays to a lower 3$^+$ level, the ground state of ^{114}Sb, with a measured lifetime τ=220 μs [16]. Representative gated coincidence spectra obtained from the present data are shown in Fig. 3.

A. Bands 1 and 2

The strong ΔI=1 transitions linking bands 1 and 2 were previously identified in Ref. [14]. The decay down to the isomeric 8$^-$ level was also established; the lowest level of band 1, assigned as 8$^-$ in Ref. [14], lies at an excitation energy of 1067 keV above the 8$^-$ isomeric state. The present work has extended band 1 to $I = 18$ and band 2 to $I = 19$.

B. Bands 3, 4, and 5

Band 4 consists of a series of 12 stretched-quadrupole transitions; a coincidence spectrum is shown in Fig. 3(b).

The three high-energy transitions constituting band 3 are also evident. The inset shows the intensity profile. Band 4 is fed over many transitions before the full intensity is reached, estimated to be $\sim$ 10% of the channel strength. The intensity drops rapidly over the lowest two transitions, indicating depopulation of the band. No definite links to the low-spin level scheme could be unambiguously assigned from the present data. As shown in Fig. 3(b), band 4 is in coincidence with the known 1185 keV 10$^-$ → 8$^-$, 453 keV 10$^-$ → 9$^-$, and 258 keV 11$^+$ → 10$^-$ transitions [14]. Apart from the lowest 560 keV transition, the band is also in coincidence with two unassigned transitions of energies 598 keV and 1495 keV. (Note that another strong 598 keV γ ray is placed in the low-spin level scheme [14]). These two transitions are in coincidence with each other and form part of the link between band 4 and the low-lying levels.

Band 5 consists of 12 stretched quadrupole transitions. As shown in the spectrum of Fig. 3(c), the band is in coincidence with low-lying 1185 keV, 750 keV, and 1131 keV transitions, except for the lowest 585 keV in-band

transition. Similar to band 4, band 5 is fed over several transitions. The maximum intensity of band 5 reaches 10% of the channel strength. The intensity of the lowest transition (585 keV) falls off, indicating feedout over the lowest two levels.

Figure 3(b) shows that the lowest member of band

TABLE IV. Gamma-ray energies, relative intensities (corrected for detector efficiency), and angular correlation data for transitions associated with bands 6 and 7 in ^{114}Sb.

E_γ (keV)[a]	I_γ (%)[b]	$\dfrac{I_\gamma(37°\text{-}79°)}{I_\gamma(79°\text{-}37°)}$	Assignment
116.4	19	—	$(9^- \to 8^-)$
139.9	147	0.5(1)	$(11^- \to 10^-)$
176.5	50	—	$(10^- \to 9^-)$
192.5	82	0.6(1)	$(13^- \to 12^-)$
235.2	103	0.5(1)	$(12^- \to 11^-)$
277.3	79	0.7(1)	$(15^- \to 14^-)$
316.5	15	—	$(11^- \to 9^-)$
322.6	54	0.6(1)	$(14^- \to 13^-)$
355.6	51	0.5(1)	$(16^- \to 15^-)$
375.3	$\equiv 100$	0.9(1)	$(12^- \to 10^-)$
376.7	31	0.5(1)	$(17^- \to 16^-)$
393.3	42	0.6(1)	$(18^- \to 17^-)$
419	< 2	—	$(20^- \to 19^-)$
423	< 2	—	$(11^- \to 12^-)^c$
428.1	30	0.9(1)	$(13^- \to 11^-)$
431	< 2	—	$(22^- \to 21^-)$
470	< 2	—	$(19^- \to 18^-)$
515.7	95	1.1(1)	$(14^- \to 13^-)$
570	< 2	—	$(21^- \to 20^-)$
600.7	65	1.0(1)	$(15^- \to 13^-)$
633.1	72	0.9(1)	$(16^- \to 14^-)$
658	< 2	—	$(12^- \to 12^-)^c$
732.6	51	0.9(1)	$(17^- \to 15^-)$
770.4	59	1.0(1)	$(18^- \to 16^-)$
802	< 2	—	$(12^-) \to 11^{+\,c}$
839.2	10	0.4(1)	$(11^-) \to 10^{-\,c}$
850.4	9	0.5(1)	$(13^-) \to 12^c$
863.7	48	1.0(1)	$(19^- \to 17^-)$
888.9	55	1.1(1)	$(20^- \to 18^-)$
988.7	45	0.9(1)	$(21^- \to 19^-)$
1001.3	56	1.1(1)	$(22^- \to 20^-)$
1102.8	32^d	$0.9(1)^d$	$(23^- \to 21^-)$
1102.9	$52^{\ d}$	$0.9(1)^d$	$(24^- \to 22^-)$
1188.5	32	—	$(26^- \to 24^-)$
1206.6	25	0.9(1)	$(25^- \to 23^-)$
1263.9	17	0.8(1)	$(28^- \to 26^-)$
1301.4	15	—	$(27^- \to 25^-)$
1336.2	13	1.4(2)	$(30^- \to 28^-)$
1390.1	7	—	$(29^- \to 27^-)$
1417.0	10	—	$(32^- \to 30^-)$
1528.2	5	—	$(34^- \to 32^-)$
1693	2	—	$(9^- \to 8^-)^c$
1869.9	30	0.8(2)	$(10^-) \to 8^{-\,c}$

[a]Energies are estimated to be accurate to ± 0.3 keV, except those quoted as integers which are accurate to ± 1 keV.
[b]Errors on the relative intensities are typically less than 5%. Bands 6 and 7 carry $\sim 15\%$ of the channel intensity.
[c]Linking transition into the known decay scheme.
[d]Doublet, value given for both transitions.

5 (585 keV) is in coincidence with band 4. Candidate linking transitions are shown in Fig. 1 as dashed lines. The first transition of energy 301 keV is clearly seen in Fig. 3(b), while the second transition of energy 357 keV is weaker. These energies are close to those expected if bands 4 and 5 are assumed to be signature partners with little signature splitting.

C. Bands 6 and 7

Bands 6 and 7 are linked by strong $\Delta I = 1$ transitions at low spin, but at higher spin collective quadrupole transitions dominate. The decay of bands 6/7 into the known low-spin levels proceeds via several pathways as shown in Fig. 2. The observed decay pattern and measured angular correlation ratios, obtained for some of the linking transitions (see Table IV) suggest a spin-parity assignment of $I^\pi = 8^-$ for the lowest level of band 6.

IV. DISCUSSION

Two mechanisms are thought to be responsible for the stabilization of enhanced quadrupole deformation in nuclei around the $Z = 50$ shell gap. The first mechanism involves the formation of the 2p-2h $\pi\{g_{7/2}^2 \otimes g_{9/2}^{-2}\}$ core state which explains deformed 0_2^+ states observed in the even tin isotopes [12]. Since the $\pi g_{7/2}$ orbital crosses the $\pi g_{9/2}$ orbital at $\beta_2 \sim 0.2$ on a standard Nilsson diagram, the formation of the 2p-2h state stabilizes the quadrupole deformation at this value. The second mechanism that induces deformation is the occupancy of the $\pi h_{11/2}[550]1/2^-$ intruder orbital from the $N = 5$ oscillator shell, which is analogous to the role played by the $N = 6$ $\nu i_{13/2}[660]1/2^+$ intruder orbital in the light rare-earth region around mass $A = 135$. Obviously, the two mechanisms for inducing deformation may reinforce each other for certain configurations. For example, on the one hand, occupation of the $\pi h_{11/2}$ intruder in the antimony isotopes ($Z = 51$) allows the formation of the deformed 0_2^+ core state, such that the deformation-driving $\pi h_{11/2} \otimes \pi\{g_{7/2}^2 \otimes g_{9/2}^{-2}\}$ proton structure is achieved. On the other hand, the occupation of positive-parity proton orbitals may perturb the deformed core state; e.g., structures of the form $\pi(+) \otimes \pi\{g_{7/2}^1 \otimes g_{9/2}^{-1}\}$ would be expected to be less deformed. The interplay between these two deformation-driving mechanisms is discussed in Ref. [7].

A. Calculated deformations

Calculations based on the total-Routhian-surface (TRS) formalism [13,17,18] have been performed for ^{114}Sb. These calculations employed a triaxial Woods-Saxon single-particle potential and a monopole pairing force residual interaction [19,20]. Self-consistent deformation parameters $(\beta_2, \beta_4, \gamma)$ for different quasiparticle configurations were evaluated at different values of the rotational frequency.

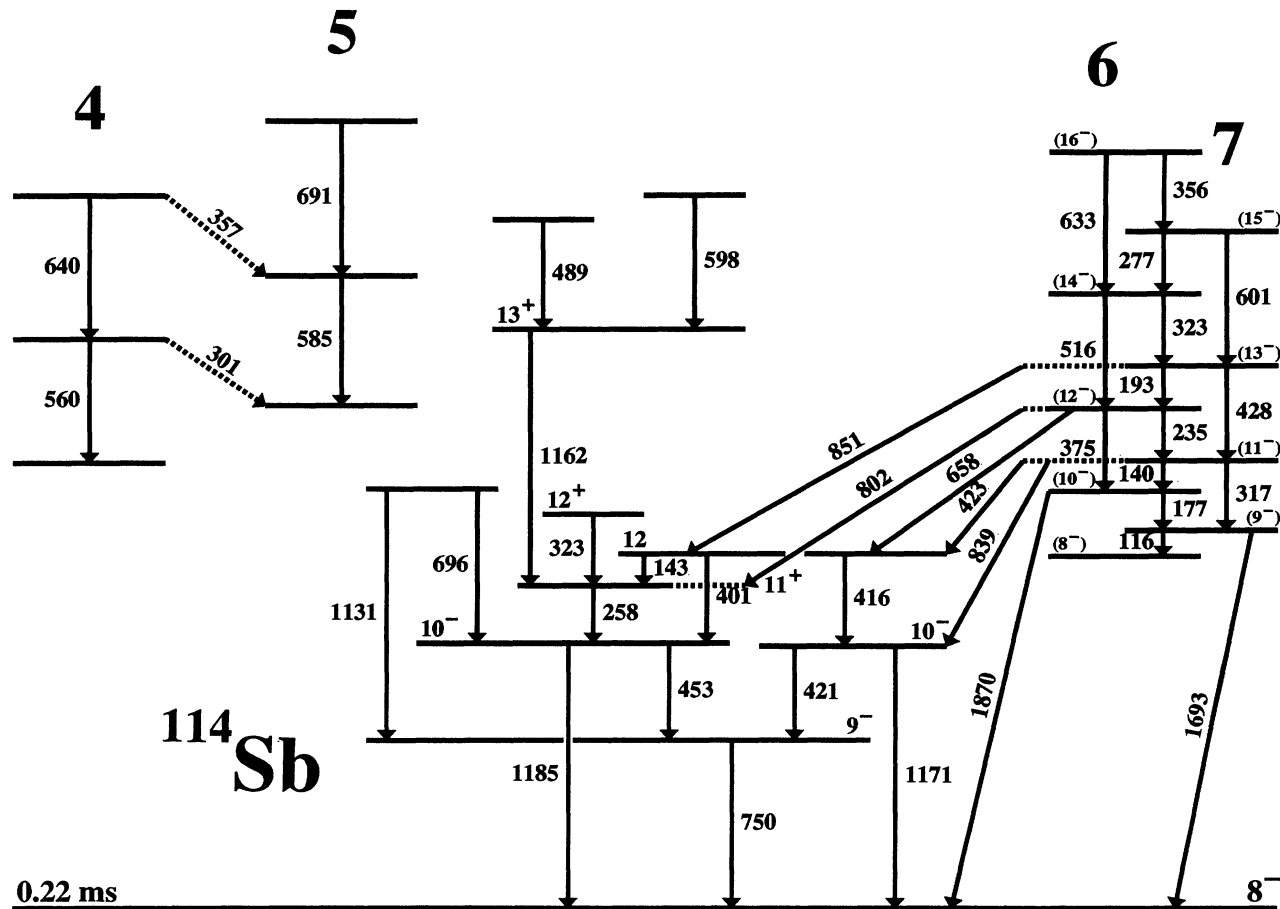Configurations of the type $\nu h_{11/2} \otimes \pi(+, \pm 1/2)$ yielded

FIG. 2. Low-spin structure of ^{114}Sb showing the decay out of bands 6 and 7. Transition energies are given in keV.

small calculated quadrupole deformation $\beta_2 \sim 0.12$ with a triaxiality of $\gamma \sim +7°$. In these configurations, $\pi(+,\pm1/2)$ refers to either $\pi g_{7/2}$ or $\pi d_{5/2}$ orbitals. In contrast, configurations involving the $[550]1/2^-$ proton intruder, e.g., $\pi h_{11/2} \otimes \nu h_{11/2}$ or $\pi h_{11/2} \otimes \nu g_{7/2}$, are predicted to possess a much larger quadrupole deformation, $\beta_2 \sim 0.24$, $\gamma \sim +5°$. The former configurations with $\beta_2 \sim 0.12$ are yrast at low spin, while the latter configurations with $\beta_2 \sim 0.24$ only become yrast for spins above $25\hbar$. At lower spins, $\sim 10\hbar$, the latter well-deformed configurations are 1–1.5 MeV above yrast.

The TRS calculations also exhibit several low-spin minima at the noncollective oblate shape $\gamma = +60°$. These configurations are shown in Table V and provide natural explanations for the low-lying 8^-, 9^-, and 11^+ states in ^{114}Sb as shown in Fig. 2. In particular, the isomeric 8^- state may be interpreted as the oblate $[\nu h_{11/2} \otimes \pi d_{5/2}]_{8^-}$ configuration. A noncollective near-yrast state is also predicted at $I^\pi = 29^+$ with large quadrupole deformation $\beta_2 = 0.28$.

In summary, the above calculations indicate two groups of near-prolate energy minima of differing deformations for configurations containing $h_{11/2}$ neutron and proton orbitals, respectively. The former minima, asso-

ciated with the $\nu h_{11/2}$ orbital, correspond to quadrupole deformation $\beta_2 \sim 0.12$; the latter, associated with the $\pi h_{11/2}$ orbital, corresponds to $\beta_2 \sim 0.24$.

B. Woods-Saxon cranking calculations

Woods-Saxon cranking calculations employing a universal triaxial Woods-Saxon single-particle potential [19,20] have been performed at the deformations predicted by the TRS calculations. Single-particle ener-

TABLE V. Calculated low-spin TRS minima at the noncollective oblate $\gamma = +60°$ shape. Energies relative to the 8^- state are shown and compared to low-lying states in ^{114}Sb.

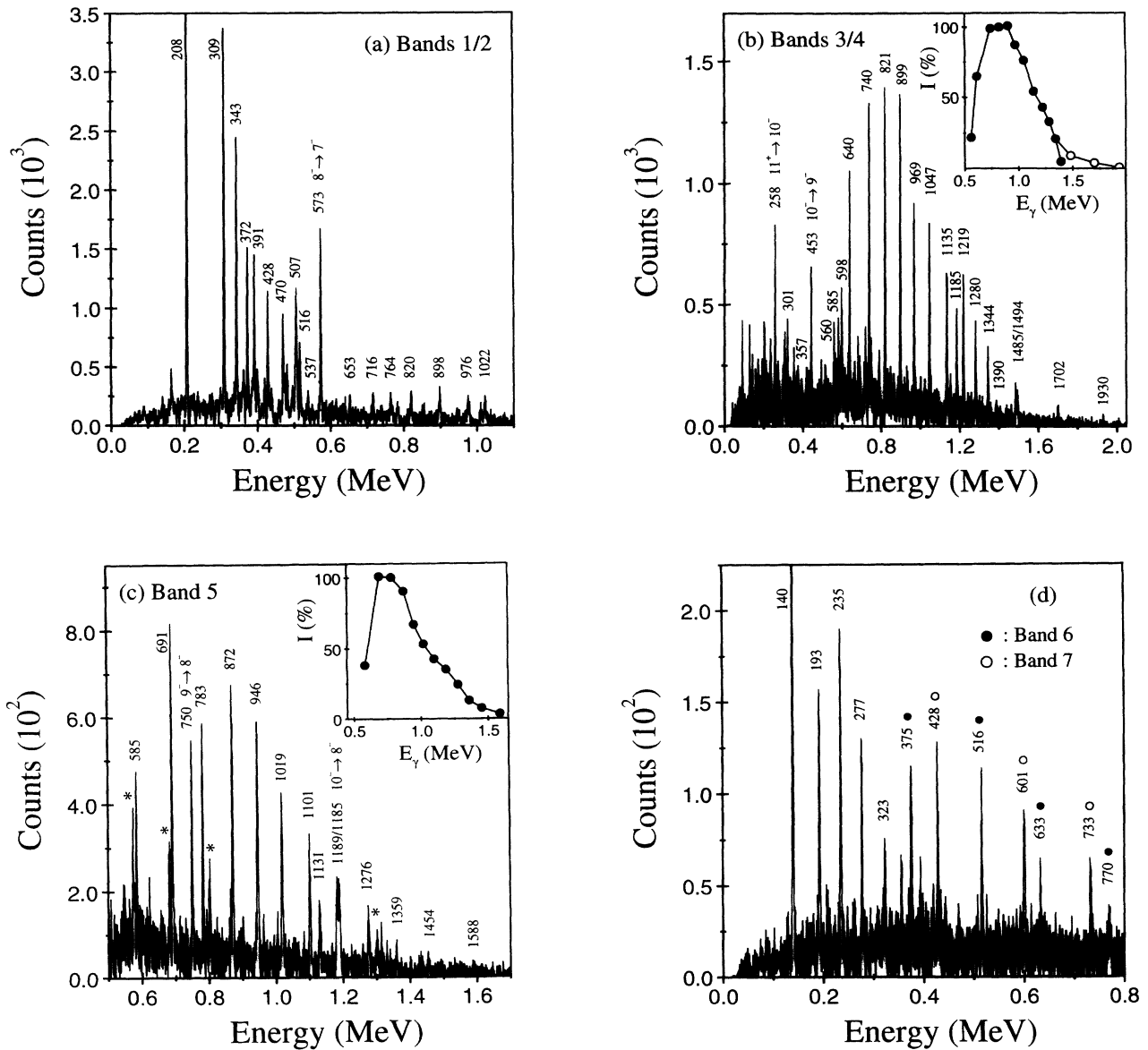| Configuration	I^π	β_2	Energy (MeV)	
			Theory	Experiment
$\nu h_{11/2} \otimes \pi d_{5/2}$	8^-	0.09	0.0	0.0
$\nu h_{11/2} \otimes \pi g_{7/2}$	9^-	0.11	0.6 ± 0.1	0.75
$\nu h_{11/2} \otimes \pi h_{11/2}$	11^+	0.12	1.8 ± 0.1	1.44

FIG. 3. Representative spectra for ^{114}Sb. Transition energies are labeled in keV. (a) Sum of gates on 494 and 1067 keV transitions that depopulate bands 1/2. (b) Sum of gates set on the 969, 1047, 1135, 1219, 1280, and 1344 keV transitions of band 4. The 598 keV and 1494 keV transitions are involved in the decay of the band to the low-spin levels. The 585 keV transition belongs to band 5, while the 301 keV and 357 keV transitions are candidate dipole transition interlinking bands 4 and 5. (c) Sum of gates set on the 691, 783, and 872 keV transitions of band 5. Contaminating lines from ^{114}Sn are marked by the stars. (d) A gate set on the 1870 keV 10^- → 8^- transition that depopulates bands 6/7.

TABLE VI. Quasiparticle crossing frequencies obtained from cranked Woods-Saxon calculations at various quadrupole deformations.

Alignment	$\hbar\omega_c$ (MeV)		
	$\beta_2 = 0.12$	$\beta_2 = 0.24$	$\beta_2 = 0.32$
$[\nu h_{11/2}]^2$	0.34	0.32	0.39
$[\nu h_{11/2}]^{2a}$	0.47	0.45	0.55
$[\nu g_{7/2}]^2$	0.66	0.85	> 0.9
$[\pi h_{11/2}]^2$	0.69	0.63	0.51
$[\pi g_{7/2}]^2$	0.47	0.66	0.85

[a]Alignment of second and third valence quasiparticles.

gies, obtained from unpaired calculations, are shown as a function of frequency in Figs. 4 and 5, respectively, for quadrupole deformations $\beta_2 = 0.12$, $\gamma = +5°$ and $\beta_2 = 0.24$, $\gamma = +5°$.

Similar calculations, including pairing, have also been performed in order to predict the alignment frequencies for specific quasiparticle pairs. The results are summarized in Table VI. Crossing frequencies are shown for deformations corresponding to the two TRS minima, as well as the experimentally deduced quadrupole deformation for an intruder band in ^{113}Sb ($\beta_2 \sim 0.32$) [5]. Calculations performed as a function of quadrupole deformation
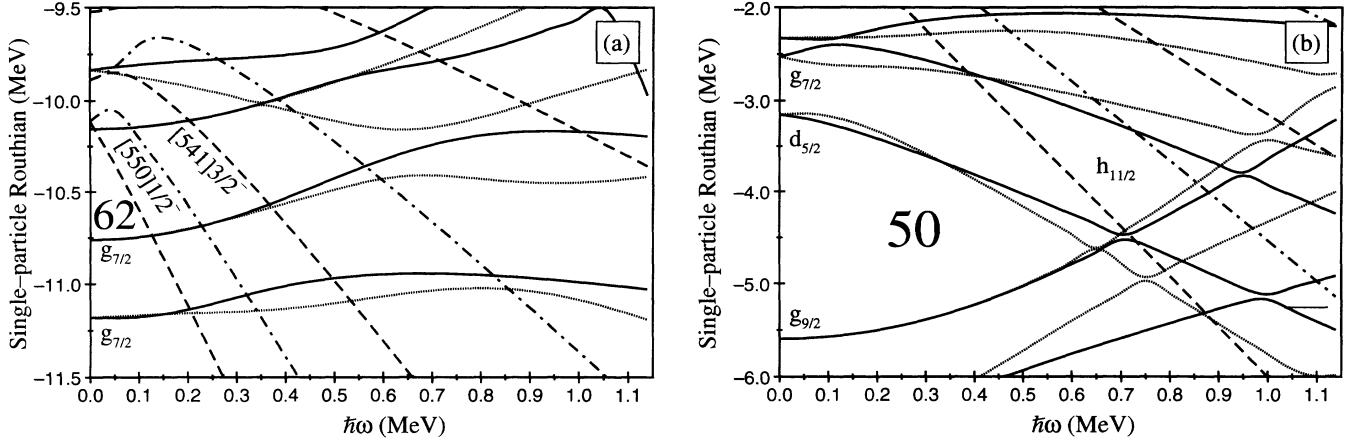
FIG. 4. Woods-Saxon single-particle energies for neutrons (a) and protons (b) calculated at a deformation $\beta_2 = 0.12$, $\beta_4 = 0.0$, and $\gamma = +5°$. The $\nu h_{11/2}$ orbitals are labeled by their asymptotic Nilsson quantum numbers.

β_2 are shown in Fig. 6 and clearly show the differing driving forces of the $h_{11/2}$ neutron and proton intruder orbitals. While the $h_{11/2}$ neutron orbital shows an energy minimum at $\beta_2 \sim 0.21$, the $h_{11/2}$ proton orbital favors $\beta_2 \sim 0.41$. It should be emphasized that these calculations show deformations favored by the single-quasiparticle orbitals, and do not necessarily represent the overall nuclear shape. The shapes predicted by the TRS calculations are more realistic.

C. Comparison with experiment

In order to compare the theoretical calculations with the band structures in ^{114}Sb, dynamic moments of inertia $\mathcal{J}^{(2)} = dI/d\omega$ ($\approx 4/\Delta E_\gamma$) are shown in Fig. 7. The dynamic moments of inertia are useful since they can be evaluated without a knowledge of level spins. It can be seen that bands 6 and 7 [Fig. 7(b)] do not show a hump at $\hbar\omega \sim 0.45$ MeV which is present in the other bands [Fig. 7(a)]. A second hump at $\hbar\omega \sim 0.65$ MeV is,

however, seen in all bands. These humps indicate that rotational alignments of pairs of particles occur at these frequencies. Band 4 splits at the top, with the extension of three high-energy transitions labeled as band 3 in Fig. 1. These high-energy transitions lead to extremely low values of the moment of inertia at high frequencies, much lower than the rigid-body value.

Experimental alignment [21] plots are shown in Fig. 8 for the bands in ^{114}Sb where they are compared to intruder bands in ^{113}Sb [5] and ^{111}In [7]. A rotational reference with Harris parameters [22] $\mathcal{J}_0 = 29.4\hbar^2$ MeV^{-1} and $\mathcal{J}_1 = 4.4\hbar^4$ MeV^{-3} has been subtracted. These values are taken from a fit to the yrast band in ^{117}I as used in Ref. [23]. In extracting the alignments for the decoupled bands 4 and 5, bandhead spins of $10\hbar$ and $11\hbar$ were assumed, respectively. The alignment of these two decoupled bands is somewhat different to that for the strongly coupled bands in ^{114}Sb. However, the alignment pattern is similar to that of the intruder bands in ^{113}Sb and ^{111}In [Fig. 8(b)].
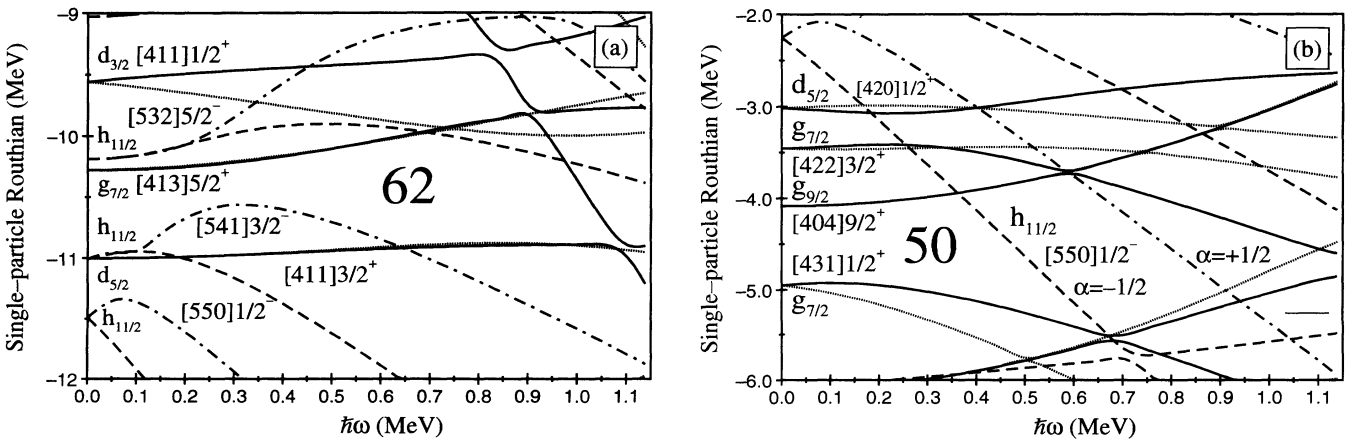

FIG. 5. Woods-Saxon single-particle energies for neutrons (a) and protons (b) calculated at a deformation $\beta_2 = 0.24$, $\beta_4 = 0.0$, and $\gamma = +5°$. Levels are labeled by their asymptotic Nilsson quantum numbers.
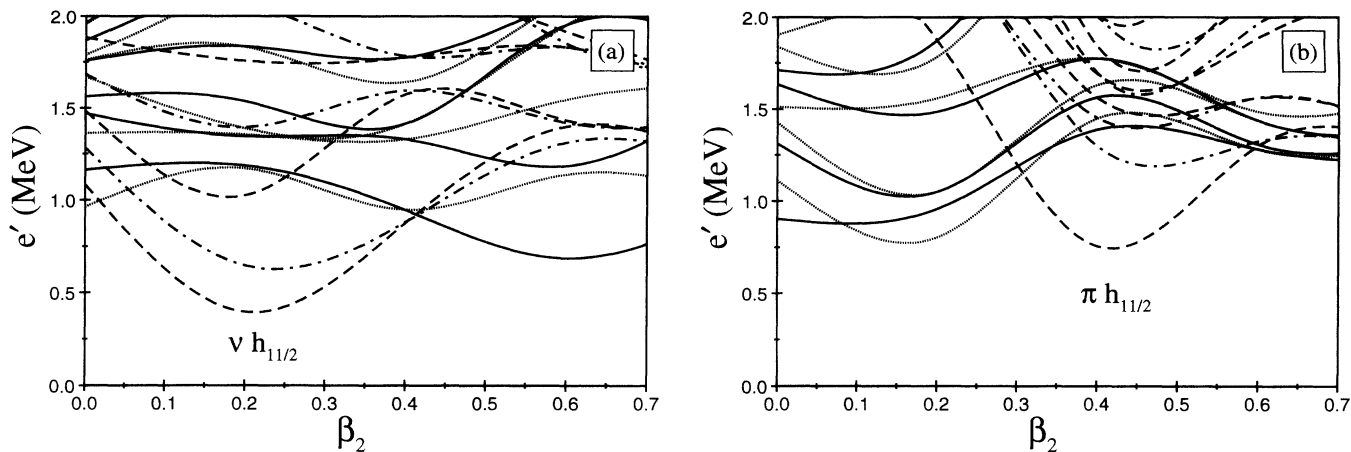
FIG. 6. Woods-Saxon quasiparticle energies calculated at $\hbar\omega = 0.25$ MeV shown as a function of quadrupole deformation for neutrons (a) and protons (b).

1. Strongly coupled bands: bands 1/2 and 6/7

Negative parity bands 1 and 2, and 6 and 7, form signature partners with little signature splitting. The pair of bands 1/2 was previously identified [14], while bands 6/7 have been established for the first time. The observation of strong $\Delta I{=}1$ transitions suggests the involvement of the $\pi g_{9/2}^{-1}$ orbital, namely, the $[404]9/2^+$ Nilsson level.

FIG. 7. Dynamic moments of inertia for bands 3, 4, and 5 (a) and bands 6/7 (b). The moment of inertia of the $\pi h_{11/2}$ intruder band of ^{113}Sb is included in (a) for comparison. The positions of rotational alignments of neutron and proton pairs are indicated.

In Ref. [14] it was suggested that bands 1/2 are based on a negative-parity $\pi g_{9/2}^{-1} \otimes \nu h_{11/2}$ configuration. However, in the present interpretation this structure is associated with bands 6/7, as discussed below. From Fig. 8(a) it can be seen that bands 1/2 carry little alignment and upbend strongly at $\hbar\omega \sim 0.45$ MeV. These two observations suggest that a rotationally aligned $\nu h_{11/2}$ particle is not involved; a larger alignment would be expected with the up-bend blocked. Such features are indeed observed for bands 6/7 which we therefore associate with the $\pi g_{9/2}^{-1} \otimes \nu h_{11/2}$ configuration. A possible configu-
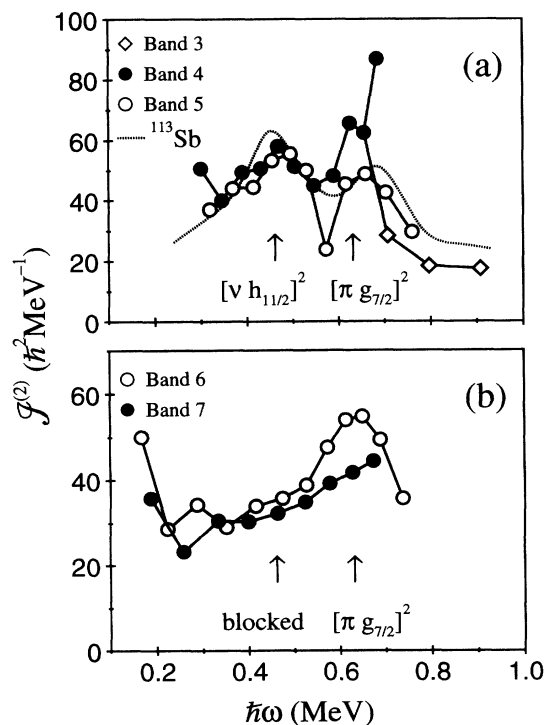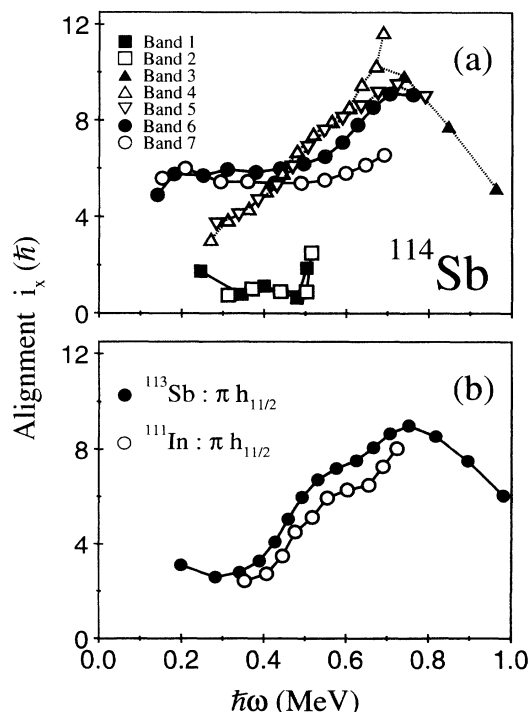

FIG. 8. Experimental alignment plots for the bands in ^{114}Sb (a) and intruder bands in ^{113}Sb and ^{111}In (b).

ration for bands 1/2 is a high-K $\pi g_{9/2}^{-1} \otimes \nu g_{7/2}$ structure involving both high-Ω proton and neutron orbitals such that the alignment is small [Fig. 8(a)]. This structure would, however, have positive parity in disagreement with the negative parity assigned in Ref. [14]. No candidate negative-parity structures showing the properties of bands 1/2 [i.e., no signature splitting and very low alignment (high K)] are evident from the cranking calculations.

The alignment i_x for bands 6/7, as shown in Fig. 8, is $(5-6)\hbar$. This value is consistent with the coupling of the high-Ω $\pi g_{9/2}^{-1}$ orbital with a low-Ω $h_{11/2}$ neutron. Relative to the Z=50 core, the $\left[\pi g_{7/2}^{2} g_{9/2}^{-1}\right]_{K=9/2}^{I=9/2} \otimes \nu h_{11/2} (\Omega = 3/2)$ configuration is thus proposed for the strongly coupled bands 6/7. Note that the deformation-driving $\pi\{g_{7/2}^{2} \otimes g_{9/2}^{-2}\}$ core state is broken in this configuration and hence a quadrupole deformation near the smaller of the TRS minima ($\beta_2 \sim 0.12$) is expected. A small signature splitting is observed between bands 6 and 7, consistent with a non-axial shape as predicted by the TRS calculations ($\gamma \sim +7°$). In fact a signature inversion occurs at a rotational frequency $\hbar\omega = 0.36$ MeV. The occupation of the $h_{11/2}$ neutron orbital will block the first rotational alignment of an $h_{11/2}$ neutron pair. This is consistent with the dynamic moment of inertia plot of Fig. 7(b), where the first hump, seen in other bands at $\hbar\omega \sim 0.45$ MeV, is absent. The second rise in the moment of inertia at $\hbar\omega \sim 0.60$ MeV may be associated with the rotational alignment of $g_{7/2}$ protons such that the high-spin configuration is $\left[\pi g_{7/2}^{2} g_{9/2}^{-1}\right]_{K=9/2}^{I=21/2} \otimes \nu h_{11/2}$.

Experimental $B(M1; I \to I-1)/B(E2; I \to I-2)$ ratios of reduced transition probabilities are shown in Fig. 9 for bands 1/2 and 6/7 in ^{114}Sb. The values obtained for the new bands 6/7 are on average 2–3 times smaller than those obtained for bands 1/2 and show a distinct signature dependence, i.e., zigzag. The higher values for bands
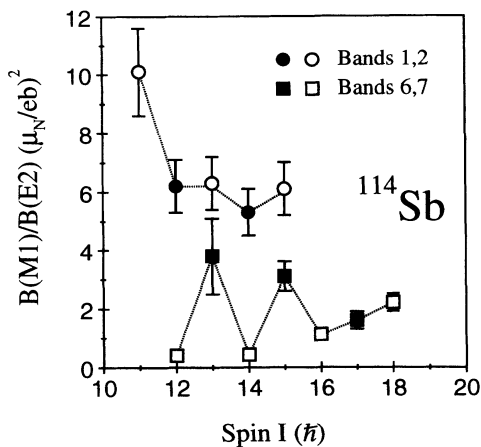

FIG. 9. Experimental $B(M1; I \to I-1)/B(E2; I \to I-2)$ ratios of reduced transition probabilities for bands 1/2 and 6/7 in ^{114}Sb. In extracting these ratios it is assumed that for the ΔI=1 transitions the multipole mixing ratio is negligible, i.e., $\delta^2 \ll 1$.

1/2 may indicate a smaller $B(E2)$ strength, and hence less collectivity; bands 1/2 are therefore not observed to such high spin. These experimental observations provide further evidence for the proposed structures of the strongly coupled bands discussed above.

2. Decoupled bands: bands 3, 4, and 5

The similarity of the moments of inertia [Fig. 7(a)] and alignment plots [Fig. 8(a)] for bands 4 and 5 strongly suggest similar structures: i.e., these bands are signature partners. The rising alignments of bands 4 and 5 shown in Fig. 8(a) is characteristic of intruder bands built on the $\pi h_{11/2}$ orbital, e.g., ^{111}In [7] and ^{113}Sb [5] shown in Fig. 8(b). If the odd proton occupies the $\pi h_{11/2}[550]1/2^-$ intruder orbital, this will allow the formation of the deformed $\pi\{g_{7/2}^{2} \otimes g_{9/2}^{-2}\}$ core state. Hence the proton structure will be able to stabilize enhanced quadrupole deformation. The appropriate single-particle diagram is thus the one for $\beta_2 = 0.24$ as shown in Fig. 5(a). It can be seen that the $\nu g_{7/2}[413]5/2^+$ orbital is at the Fermi surface for N=63. This orbital shows little or no signature splitting below a frequency $\hbar\omega = 0.70$ MeV. The proposed structure for bands 4/5 is thus $\pi h_{11/2} \otimes \nu g_{7/2}$ coupled to the deformed $\pi\{g_{7/2}^{2} \otimes g_{9/2}^{-2}\}$ core state. Bands 4/5 can therefore be thought of as coupling the single intruder band in ^{113}Sb [5] to both signatures of a $g_{7/2}$ neutron orbital. The similarity of the moments of inertia and alignments reinforces this view. The extra $g_{7/2}$ neutron orbital plays the role of a spectator.

With this basic configuration for bands 4/5, the first hump in the moment-of-inertia plot of Fig. 7(a) at $\hbar\omega \sim 0.45$ MeV can now be interpreted as the rotational alignment of a pair of $h_{11/2}$ neutrons. Similarly, the second hump at $\hbar\omega \sim 0.65$ MeV can be associated with the rotational alignment of a pair of $g_{7/2}$ protons, as also seen for bands 6/7. The first neutron crossing at $\hbar\omega \sim 0.45$ MeV is somewhat higher than the predictions shown in Table VI. Similar delayed crossings of $h_{11/2}$ neutrons in bands built on the $\pi h_{11/2}[550]1/2^-$ intruder orbital have been observed in several neighboring nuclei, including ^{113}Sb [5], ^{111}In [7], and ^{117}I [23]. This effect has been attributed to strong neutron-proton residual interactions between the $\pi h_{11/2}$ intruder orbital and the aligning $\nu h_{11/2}$ particles [5,24].

No definite interlinking dipole transitions could be established between bands 4 and 5 although tentative links are shown in Fig. 2 and Fig. 3(b). However, the $B(M1)$ rate would not be expected to be large for the proposed $\pi h_{11/2} \otimes \nu g_{7/2}$ configuration since the resultant magnetic-moment vector, dominated by the rotationally aligned $h_{11/2}$ proton, will point in a similar direction to the spin vector. Furthermore, the predicted well-deformed shape ($\beta_2 \sim 0.24$) would enhance the collective in-band $B(E2)$ strength such that the $E2$ decay dominates.

Band 4 appears to split at the top where the final transition (1390 keV) is parallel to the high-energy 1485 keV transition. In fact three high-energy transitions, labeled as band 3 in Fig. 1, feed into band 4. The relatively large energy spacings of the transitions in band 3 lead

to extremely low values of the dynamic moment of inertia [Fig. 7(a)] and a drop in alignment [Fig. 8(a)]. A similar falling alignment at high spin is observed in the intruder band of ^{113}Sb [Fig. 8(b)]. Unusually low values of the dynamic moment of inertia at high spin have also been observed in several other nuclei, including ^{109}Sb [3], where the values drop to $1/2$–$1/3$ of the rigid body value. Such behavior has been taken as evidence for a form of band termination where the nucleus smoothly changes shape from prolate to oblate over many transitions. Indeed, with few valence nucleons outside the $Z = N = 50$ doubly magic shell closure, such effects are to be expected in this mass region.

V. CONCLUSIONS

The decay scheme of ^{114}Sb has been extended to high spin where collective rotational bands dominate. Two pairs of signature-partner bands have been identified. One pair shows interlinking dipole transitions at low spin and is associated with a $\pi g_{9/2} \otimes \nu h_{11/2}$ structure. The second pair is interpreted in terms of a $\pi h_{11/2} \otimes \nu g_{7/2}$ configuration with possible enhanced deformation. The observation of long cascades of transitions extending to high spin has recently burgeoned in the mass $A \sim 110$ region.

[1] J. Bron, W.H.A. Hesselink, A. van Poelgeest, J.J.A. Zalmstra, M.J. Uitzinger, H. Verheul, K. Heyde, M. Waroquier, H. Vincx, and P. van Isacker, Nucl. Phys. **A318**, 335 (1979).

[2] V.P. Janzen *et al.*, in *Proceedings of the International Conference on Nuclear Structure at High Angular Momentum*, Ottawa, 1992, edited by J.C. Waddington and D. Ward (AECL Research, Chalk River, 1992), AECL Report No. 10613, Vol. 2, p. 333.

[3] V.P. Janzen, D.R. LaFosse, H. Schnare, D.B. Fossan, A. Galindo-Uribarri, S.M. Mullins, E.S. Paul, L. Persson, S. Pilotte, D.C. Radford, H. Timmers, J.C. Waddington, R. Wadsworth, D. Ward, J.N. Wilson, and R. Wyss, Phys. Rev. Lett. **72**, 1160 (1994).

[4] D.R. LaFosse, D.B. Fossan, J.R. Hughes, Y. Liang, P. Vaska, M.P. Waring, J.-y. Zhang, R.M. Clark, R. Wadsworth, S.A. Forbes, E.S. Paul, V.P. Janzen, A. Galindo-Uribarri, D.C. Radford, D. Ward, S.M. Mullins, D. Prévost, and G. Zwartz, Phys. Rev. C **50**, 1819 (1994).

[5] V.P. Janzen, H.R. Andrews, B. Haas, D.C. Radford, D. Ward, A. Omar, D. Prévost, M. Sawicki, P. Unrau, J.C. Waddington, T.E. Drake, A. Galindo-Uribarri, and R. Wyss, Phys. Rev. Lett. **70**, 1065 (1993).

[6] D.R. LaFosse, D.B. Fossan, J.R. Hughes, Y. Liang, P. Vaska, M.P. Waring, and J.-y. Zhang, Phys. Rev. Lett. **69**, 1332 (1992).

[7] S.M. Mullins, V.P. Janzen, P. Vaska, G. Hackman, D.B. Fossan, D.R. LaFosse, E.S. Paul, D. Prévost, H. Schnare, J.C. Waddington, R. Wadsworth, and M.P. Waring, Phys. Lett. B **318**, 592 (1993).

[8] R. Wadsworth, H.R. Andrews, C.W. Beausang, R.M. Clark, D.B. Fossan, A. Galindo-Uribarri, I.M. Hibbert, K. Hauschild, J.R. Hughes, V.P. Janzen, D.R. LaFosse, S.M. Mullins, E.S. Paul, D.C. Radford, H. Schnare, P. Vaska, D. Ward, and I. Ragnarsson, Phys. Rev. C **50**, 483 (1994).

[9] R. Wadsworth, H.R. Andrews, R.M. Clark, D.B. Fossan, A. Galindo-Uribarri, V.P. Janzen, J.R. Hughes, D.R. LaFosse, S.M. Mullins, E.S. Paul, D.C. Radford, P. Vaska, M.P. Waring, D. Ward, J.N. Wilson, and R. Wyss, Nucl. Phys. **A559**, 461 (1993).

[10] E.S. Paul, C.W. Beausang, S.A. Forbes, S.J. Gale, A.N. James, P.M. Jones, M.J. Joyce, H.R. Andrews,

V.P. Janzen, D.C. Radford, D. Ward, R.M. Clark, K. Hauschild, I.M. Hibbert, R. Wadsworth, R.A. Cunningham, J. Simpson, T. Davinson, R.D. Page, P.J. Sellin, P.J. Woods, D.B. Fossan, D.R. LaFosse, H. Schnare, M.P. Waring, A. Gizon, J. Gizon, T.E. Drake, J. DeGraaf, and S. Pilotte, Phys. Rev. C **50**, 698 (1994).

[11] E.S. Paul, C.W. Beausang, R.M. Clark, R.A. Cunningham, T. Davinson, S.A. Forbes, D.B. Fossan, S.J. Gale, A. Gizon, J. Gizon, K. Hauschild, I.M. Hibbert, A.N. James, P.M. Jones, M.J. Joyce, D.R. LaFosse, R.D. Page, H. Schnare, P.J. Sellin, J. Simpson, R. Wadsworth, M.P. Waring, and P.J. Woods, Phys. Rev. C **48**, R490 (1993).

[12] K. Heyde, P. Van Isacker, R.F Casten, and J.L. Wood, Phys. Lett. **155B**, 303 (1985).

[13] R. Wyss, J. Nyberg, A. Johnson, R. Bengtsson, and W. Nazarewicz, Phys. Lett. B **215**, 211 (1988).

[14] R. Duffait, J. van Maldeghem, A. Charvet, J. Sau, K. Heyde, A. Emsallem, M. Meyer, R. Béraud, J. Tréherne, and J. Genevey, Z. Phys. A **307**, 259 (1982).

[15] K.S. Krane, R.M. Steffen, and R.M. Wheeler, Nuclear Data Tables A **11**, 351 (1973).

[16] R. Kamermans, H.W. Jongsma, T.J. Ketel, R. van der Wey, and H. Verheul, Nucl. Phys. **A266**, 346 (1976).

[17] W. Nazarewicz, G.A. Leander, and J. Dudek, Nucl. Phys. **A467**, 437 (1987).

[18] W. Nazarewicz, R. Wyss, and A. Johnson, Nucl. Phys. **A503**, 285 (1989).

[19] W. Nazarewicz, J. Dudek, R. Bengtsson, and I. Ragnarsson, Nucl. Phys. **A435**, 397 (1985).

[20] S. Cwiok, J. Dudek, W. Nazarewicz, W. Skalski, and T. Werner, Comput. Phys. Commun. **46**, 379 (1987).

[21] R. Bengtsson and S. Frauendorf, Nucl. Phys. **A327**, 139 (1979).

[22] S.M. Harris, Phys. Rev. **138**, B509 (1965).

[23] E.S. Paul, M.P. Waring, R.M. Clark, S.A. Forbes, D.B. Fossan, J.R. Hughes, D.R. LaFosse, Y. Liang, R. Ma, P. Vaska, and R. Wadsworth, Phys. Rev. C **45**, R2531 (1992).

[24] R. Wyss and A. Johnson, in *Proceedings of the International Conference on High-Spin Physics and Gamma-Soft Nuclei*, Pittsburgh 1990, edited by J.X. Saladin *et al.* (World Scientific, Singapore, 1991), p. 123.